metals

Article

Effect of Alternating Magnetic Field Treatment on the Friction/Wear Resistance of 20Cr2Ni4A Under Lubricated Conditions

Sufyan Akram [1], Mose Bevilacqua [1], Anatolii Babutskyi [1,2,†] and Andreas Chrysanthou [1,*]

[1] School of Physics, Engineering and Computer Science, University of Hertfordshire, College Lane, Hatfield AL10 9AB, Herts, UK
[2] G.S. Pysarenko Institute for Problems of Strength, National Academy of Sciences of Ukraine, 01014 Kyiv, Ukraine
* Correspondence: a.chrysanthou@herts.ac.uk
† Deceased.

Abstract: High-strength nickel–chromium steel (20Cr2Ni4A) is typically used in bearing applications. Alternating magnetic field treatment, which is based on the use of a magnetiser, and which is fast and cost-effective in comparison to conventional processes, was applied to the material to improve its wear resistance. The results of pin-on-disc wear testing using a AISI 52100 alloy counter pin revealed a decrease in the specific wear rate of the treated samples by 58% and a reduction in the value of the coefficient of friction by 28%. X-ray diffraction analysis showed a small increase in the amount of martensite and higher surface compressive residual stresses by 28% leading to improved hardness. The observed changes were not induced thermally. The volume expansion by the formation of martensite was achieved at near room temperature and led to a further increase in compressive residual stresses. The significance of this study is that the improvement in the properties was achieved at a current density value that was two orders of magnitude higher than the threshold for phase transformation and dislocation movement. The reasons for the effect of the alternating magnetic field treatment on the friction and wear properties are discussed in terms of the contribution of the magnetic field to the austenite-to-martensite phase transformation and the interaction between the magnetic domain walls and dislocations.

Keywords: alternating magnetic field treatment; bearing steel

Academic Editor: Zhengyi Jiang

Received: 2 December 2024
Revised: 3 January 2025
Accepted: 7 January 2025
Published: 14 January 2025

Citation: Akram, S.; Bevilacqua, M.; Babutskyi, A.; Chrysanthou, A. Effect of Alternating Magnetic Field Treatment on the Friction/Wear Resistance of 20Cr2Ni4A Under Lubricated Conditions. *Metals* **2025**, *15*, 69. https://doi.org/10.3390/met15010069

1. Introduction

AISI 20Cr2Ni4A alloy is a high-strength nickel–chromium (Ni-Cr) steel that is widely used for bearing applications due to its high strength, hardness, toughness and wear resistance [1–3]. However, under extreme working conditions such as high pressure, bearing speed and temperature, the rolling contact fatigue failure of the alloy may be accelerated [4]. The failure of bearings can cause damage to machinery, leading to performance degradation in systems [5]. Therefore, extending the service life of the alloy is critical to increasing the lifetime of machinery. Traditional methods to improve the wear resistance of bearing steels include the use of shot-peening, which introduces compressive residual stresses at the surface [6]. Other popular methods involve surface hardening by the chemical modification of the surface; such methods include carburising [7] as well as nitriding [8] and carbonitriding. Ion implantation of 52100 steel with carbon has also been shown to improve wear resistance [9], while techniques like laser glazing lead to the formation of a harder surface by fast heating and cooling [10]. During recent years, research investigations have reported on the treatment of alloys by exposing them to high magnetic fields and have

demonstrated increases in fatigue resistance [11–14] and hardness [15,16]. These techniques have also led to improvements in tribological properties [17,18] by extending the level of surface hardness and compressive surface stress. Tests conducted by Snegovskij and Uvarov [19] showed that by treating marine ship propellers with a pulsed magnetic field of 10^6 A/m, the cavitation wear resistance after testing under real life conditions increased by up to two times compared to that of the reference samples. However, it must be noted that there are studies in the literature where the effect on wear has been detrimental. For example, Hiratsuka and Sasada [20] reported an increase in the wear rate of Fe while subjected to a static magnetic field while undergoing a pin-on-disc test using Cu and Zn pins in air. Their results indicated that the applied magnetic field led to the refinement and oxidation of the wear debris that accumulated in areas, causing an increase in the wear rate during rubbing with the substrate. Beneficial effects were reported by Babutskyi et al. [18], who observed that the value of the coefficient of friction of the AISI 52100 steel that had undergone pulsed magnetic treatment was reduced by 13% compared with that of the reference specimens. The authors [18] attributed the improvement in the friction and wear properties to a decrease in the surface residual stresses and to the destabilisation of the retained austenitic phase in the alloy. A similar drop in the value of the coefficient of friction (by 16.4%) of AISI 1045 steel was also reported by Xi et al. [21], who applied a pulsed magnetic field of 32 mT to the material for 30 s prior to the friction wear tests. In addition, following the treatment, there was an improvement in the Vickers microhardness by 8%. The improvement in the wear and friction properties was attributed to a 16.5% increase in the dislocation density, which was determined using the Williamson–Hall method. X-ray diffraction (XRD) analysis and microstructural observations also showed a decrease in the average grain size of the treated samples. Optical microscopy observations revealed that the treated samples displayed finer ferrite crystals than the untreated samples did; this effect was attributed to the influence of magnetostriction.

The application of external magnetic fields as a processing technique is currently gaining interest. While there has been much interest in the use of pulsed magnetic treatment, to date, there has been little research involving alternating magnetic field (AMF) treatment and, indeed, no research work on its application for alloys in bearing applications has been conducted. AMF treatment is cost-effective as it uses simpler equipment and can be speedier compared to some traditional techniques. However, it operates at a lower current density (which is the most influential parameter) than pulsed magnetic treatment and it can be a challenge for AMF to achieve the necessary transformations for improved mechanical properties. The research presented in this paper investigates the effect of AMF treatment on the tribological properties of a typical material used for sliding contact bearings like 20Cr2Ni4A high-strength Ni-Cr steel. Sliding contact friction and wear tests were conducted using a pin-on-disc tribometer. Scanning electron microscopy (SEM) was employed to examine the wear scar tracks, while atomic force microscopy (AFM) was performed to elucidate the effects of the AMF treatment. Analysis of the residual stress state and phase identification were conducted for untreated and treated samples using XRD. In addition, mechanical tests like nano- and microhardness tests were performed on samples prior to and after treatment.

2. Materials and Methods

In the present study, the friction and wear properties of AMF-treated and untreated high-strength Ni-Cr steel were investigated. Three samples in each condition (untreated and treated) were prepared from loose-bearing high-strength Ni-Cr steel (25.4 mm diameter) for pin-on-disc wear testing. The nominal composition of the high-strength Ni-Cr steel that was used is shown in Table 1.

Table 1. Chemical composition of high-strength Ni-Cr (20Cr2Ni4A) steel. Adapted from Ref. [3].

Composition	C	Si	Mn	P	S	Cr	Ni	Fe
Percentage (wt.%)	0.20	0.24	0.37	0.011	<0.005	1.33	3.41	Bal.

An alternating magnetic field was applied to specimens by placing them between two magnetiser cores. Figure 1a schematically shows the magnetic field direction in the case of pin-on-disc samples. A Hirst GM08 Gaussmeter (Hirst, Falmouth, Cornwall, UK) was used to measure the magnetic flux density, recorded by means of a Picoscope 4224 digital oscilloscope (Pico Technology, St. Neots, Cambridgeshire, UK) as shown in Figure 1b. The maximum recorded value during the AMF treatment was 1.24 T. A K-type thermocouple was used to measure the sample temperature during the AMF treatment. A thermocouple attached to the centre of the circular surface of the specimen measured the average maximum temperature increase to be 15.2 °C during AMF treatment.

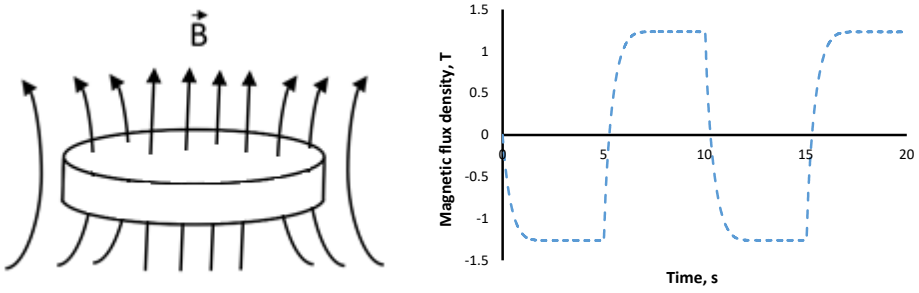

(**a**) (**b**)

Figure 1. Schematic diagrams of (**a**) the AMF treatment for the pin-on-disc sample and (**b**) a plot of the magnetic flux density against time during AMF treatment.

Pin-on-disc tests were performed to investigate the wear resistance and sliding properties at the surface of samples. A POD 2 pin-on-disc tester supplied by Teer Coatings Ltd. (Teer Coatings Ltd., Droitwich, Worcestershire, UK) shown schematically in Figure 2 was used to evaluate the wear and friction properties of AMF-treated and untreated high-strength Ni-Cr steel. The tests were conducted under lubrication using sunflower oil at an ambient temperature of 22 °C. A 3 mL layer of sunflower oil was applied as a lubricant using a pipette. Vegetable oils have been widely utilised in tribological studies due to their sustainability and environmental friendliness. Recent research [22] has shown that they can outperform conventional oils in certain applications. A sliding speed of 50 mm/s under a vertical load of 20 N was applied for 1 h during the pin-on-disc test, which was performed according to the ASTM 99-95a standard [23]. In a pin-on-disc test, the coefficient of friction (COF) is determined by dividing the tangential force by the normal load exerted on the pin, as shown in Equation (1) below:

$$COF = \frac{Tangential\ Force}{Normal\ Load} \quad (1)$$

The pin-on-disc samples were machined from a 25.4 mm diameter bar and cut to 3.1 mm thickness. The contact bearing pin was 5 mm diameter spherical AISI 52100 bearing steel with an HRC hardness of 61–63 and a surface roughness of 20 nm. The disc samples were first ground using 180-grit silicon carbide paper. Polishing was then performed sequentially, starting with Abracloth and a 9 µm diamond suspension, followed by Planocloth with a 3 µm diamond suspension. The final polishing step utilised a Multicloth polishing pad, resulting in a surface roughness of approximately 15 nm. The specific wear rates of the samples were calculated using a precision digital scale with an accuracy of ±0.1 mg by

measuring the weight before and after the pin-on-disc wear tests. Equation (2) was used to calculate the specific wear rates of the untreated and AMF-treated discs:

$$W = \frac{\Delta w}{L \rho F} \tag{2}$$

where W represents the specific wear rate in mm^3/Nm, Δw is the weight loss in grams, L is the sliding distance in m, ρ is the density of the worn material in g/mm^3 and F is the applied load in N. SEM examination of the wear scars was conducted using a JEOL JSM-5700F scanning electron microscope (JEOL UK, Welwyn Garden City, UK) that was operated at 20 kV. Atomic Force Microscopy (AFM) was carried out with an Easyscan 2 Nanosurf atomic force microscope equipped with a Tap190Al-G cantilever probe (Nanosurf UK, Bracknell, UK). The samples that had undergone pin-on-disc testing were further analysed using AFM by studying the topography of the wear tracks and their surface roughness.

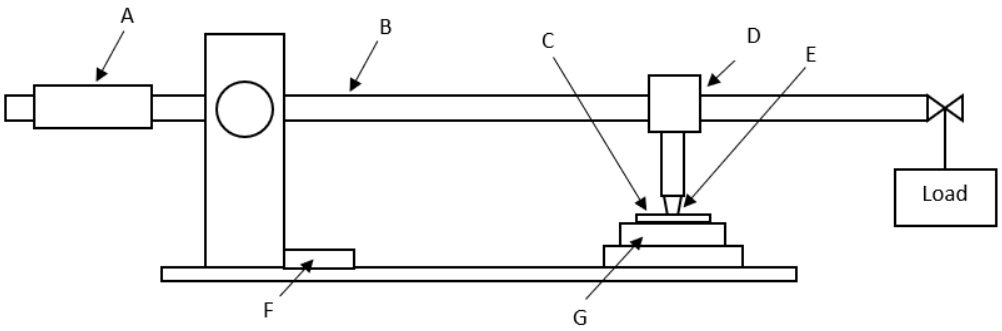

Figure 2. Diagram of POD 2 pin-on-disc tester: (A) balance weight, (B) load beam, (C) sample, (D) load cell, (E) wear pin (ball) and holder, (F) wear track radius micrometre adjustment, and (G) rotating sample table.

Three samples in each condition (untreated and treated) with the same geometry as those used for the pin-on-disc tests were also used for XRD analysis and for micro- and nanohardness testing. Vickers microhardness tests were conducted using a Struers Dura 20 microhardness tester (Struers Ltd., Rotherham, UK) with a load of 10 N. A total of sixty indentations along two perpendicular diameters within the same sample were performed. For nanoindentation testing, a Micro Materials NanoTest Vantage Platform 5 equipped with a Diamond Berkovich indenter (Micro Materials Ltd., Wrexham, UK) was used to perform the measurements. A total of 100 indents were performed using a load of 50 mN along with a load-hold time of 10 s, a dwell period of 20 s and an unloading time of 5 s. Indentations were performed using a 10 by 10 grid matrix with 100 μm spacing between each indentation. Furthermore, the H/E^2 ratio (where H represents hardness and E the elastic modulus) was calculated to characterise the resistance to plastic deformation. The elastic modulus determined by nanoindentation tests can be calculated using Equation (3):

$$E = \frac{1 - {v_s}^2}{\frac{1}{E_r} - \frac{1-{v_i}^2}{E_i}} \tag{3}$$

where E represents the elastic modulus of the sample, v_s and v_i are the Poisson's ratio of the sample and the Berkovich indenter, respectively, E_i is the elastic modulus of the indenter and E_r is the reduced modulus of the sample after indentation.

Phase changes and changes in the residual stress of the high-strength Ni-Cr steel were obtained by using a Bruker D8 Advance X-ray diffractometer (Bruker UK Ltd., Coventry, UK) that was equipped with a Cu anode (Kα, λ = 1.540549 Å). The tube voltage and current were set at 40 kV and 40 mA. XRD phase identification was conducted in the range of 20–90° with a step size of 0.019°. Using the Bruker TOPAS version 6 software,

Rietveld refinement was conducted to determine changes in the crystalline structure before and after AMF treatment. For residual stress analysis, the peak of the (310) plane was evaluated at 2θ = 116°. The determination of the residual stresses was carried out using the Sliding Gravity method, which is the preferred method for industrial products [24]. Leptos software version 7.9 was used for analysing the residual stress data.

Numerical modelling of the magnetic field and the resulting eddy current distribution was therefore undertaken to obtain the value of the current density during the AMF treatment. This was carried out by using QuickField 6 software (Tera Analysis, Svendborg, Denmark). The software utilised a 2D formulation to solve the transient magnetic field problem. Table 2 presents the physical properties employed for the finite element analysis.

Table 2. Physical properties of materials used during simulation modelling.

Property	Core (Steel)	Spacer (Steel)	Winding Wire (Copper)	Ni-Cr Steel Sample	Surrounding Air
Electrical conductivity, MS/m	10	10	56	10	0
Relative permeability	B-H curve *	B-H curve *	1	B-H curve *	1

* The value of the magnetic flux density vs. magnetic field strength (B-H) curve for steel was taken from [25].

The full current time variation, $I(t)$, passing through a single turn of magnetizer windings can be calculated by Equation (4):

$$I(t) = I_0 sign\ (sin\ (2\pi t/T)) \quad (4)$$

where t is the time at any instant and T represents the duration during which the magnetic field operates in both directions of the magnetizer; the value of T in the present work was 10 s as the magnetic field was altered every 5 s. A schematic representation of the model that was used in the simulation is shown in Figure 1a. To obtain the value of I_0, the fit between the calculated and recorded profiles of the magnetic flux density from the magnetizer in the absence of a sample was optimised. In Figure 1b, the magnetic flux density was observed to be 1.24 T. The modelling process involved simulating the magnetizer with a high-strength Ni-Cr steel sample placed at its centre. Figure 3 illustrates a quarter-section geometric model representing the treatment configuration employed for numerical simulation.

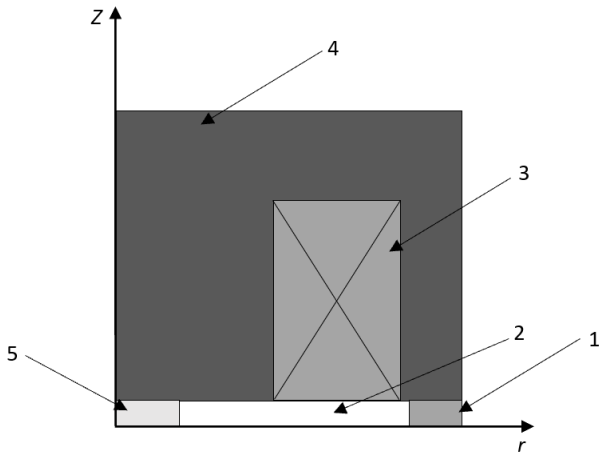

Figure 3. Schematic representation of the model employed in the simulation: 1, spacer; 2, air; 3, windings (comprising 70 turns); 4, air magnetizer core; and 5, disc sample.

3. Results

The pin-on-disc test results for the AMF-treated and untreated high-strength Ni-Cr steel are shown in Figure 4a, while the specific wear rate and the average coefficient of friction values are displayed in Figure 4b. These results show that the average value of the coefficient of friction of the AMF-treated samples had decreased in comparison with that of the untreated samples. Table 3 presents the microhardness results along with the average width of the wear scars and data of the residual stress. Following the AMF treatment, the average coefficient of friction value was lower by 28%, while the specific wear rate decreased by 58%. The residual stress results in Table 3 show that there was an increase in compressive residual stress by 28% following the AMF treatment. In addition, a slight increase in the average microhardness was observed following the treatment.

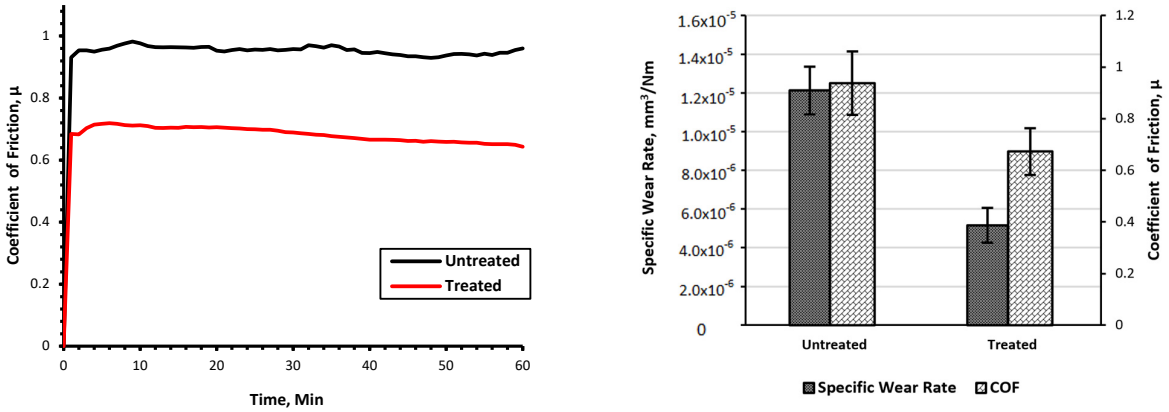

(**a**) (**b**)

Figure 4. (**a**) Variation in the coefficient of friction for untreated and AMF-treated disc specimens of high-strength Ni-Cr steel; (**b**) specific wear rate and the average coefficient of friction for the untreated and AMF-treated conditions.

Table 3. Mean (M) and mean square deviation (MSD) results of microhardness, wear track width, surface roughness and residual stress.

		[1] Microhardness, HV		[2] Wear Scar Width, μm		[3] Average Roughness, R_a, nm		[4] Residual Stress, MPa	
		M	**MSD**	**M**	**MSD**	**M**	**MSD**	**M**	**MSD**
High-strength Ni-Cr Steel	Untreated	789.8	13.3	145.2	5	25.41	±0.41	−301.9	±62.4
	Treated	796	9.9	112.5	6.9	7.91	±0.39	−385	±12.6

[1] Average values of 60 indentations per sample (3 samples); [2] average values of 3 samples measured across the wear scar width; [3] average values of 5 measurements per sample (1 measurement in each quadrant out of 3 samples); [4] average values of 5 measurements per sample (3 samples).

Analysis of the wear behaviour of the untreated and AMF-treated pin-on-disc surfaces was undertaken by conducting SEM and AFM observations of the worn surfaces. Figure 5 presents the results of SEM examination of the surfaces that experienced wear; it also displays the wear scar width for samples in the untreated and treated conditions. Figure 6 shows the three-dimensional topography that was obtained by AFM of the wear tracks for the tested specimens. The AFM and SEM results show that the treated sample displayed shallower grooves within the wear track compared with the untreated specimen. It is apparent that the AMF treatment resulted in a decrease in the wear track width and of the surface roughness by an average of 23% and 69%, respectively.

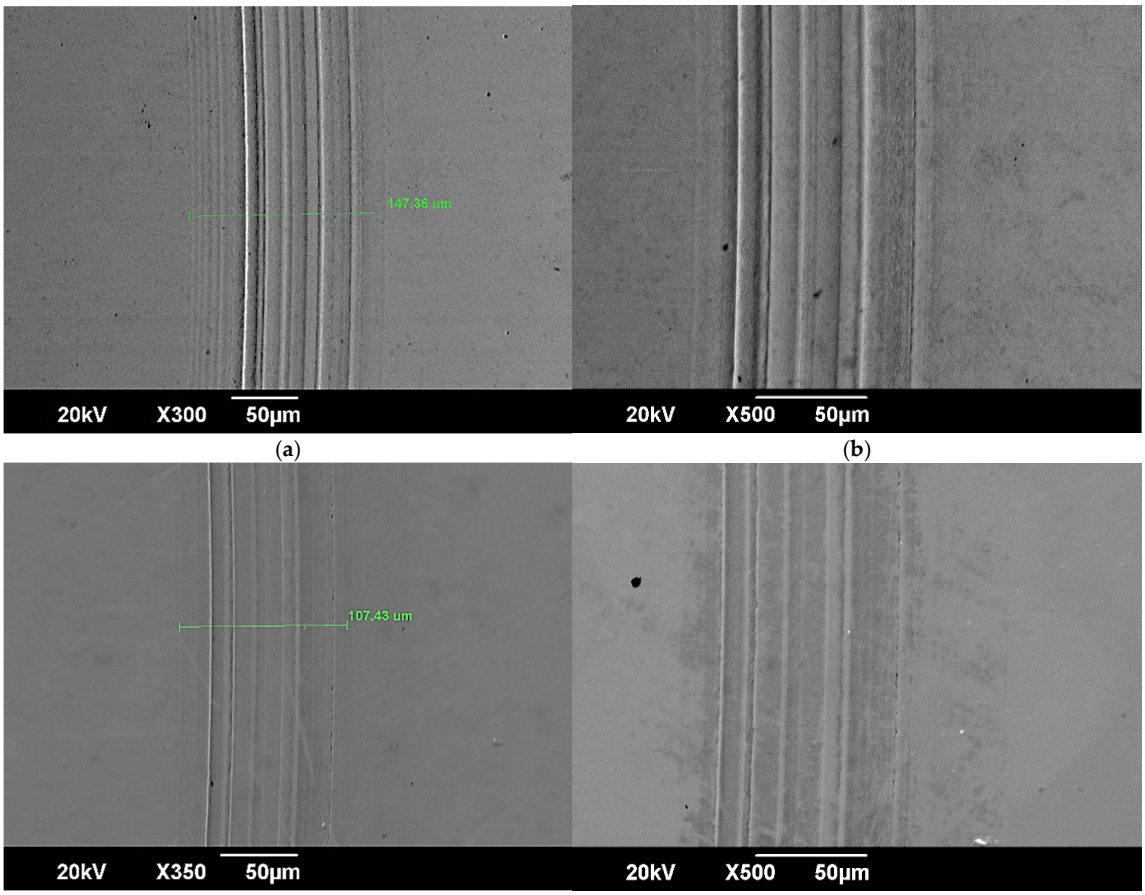

(**a**) (**b**)

(**c**) (**d**)

Figure 5. SEM wear tracks of the surface of untreated (**a**,**b**) and treated (**c**,**d**) high-strength Ni-Cr steel after 1 h of pin-on-disc testing.

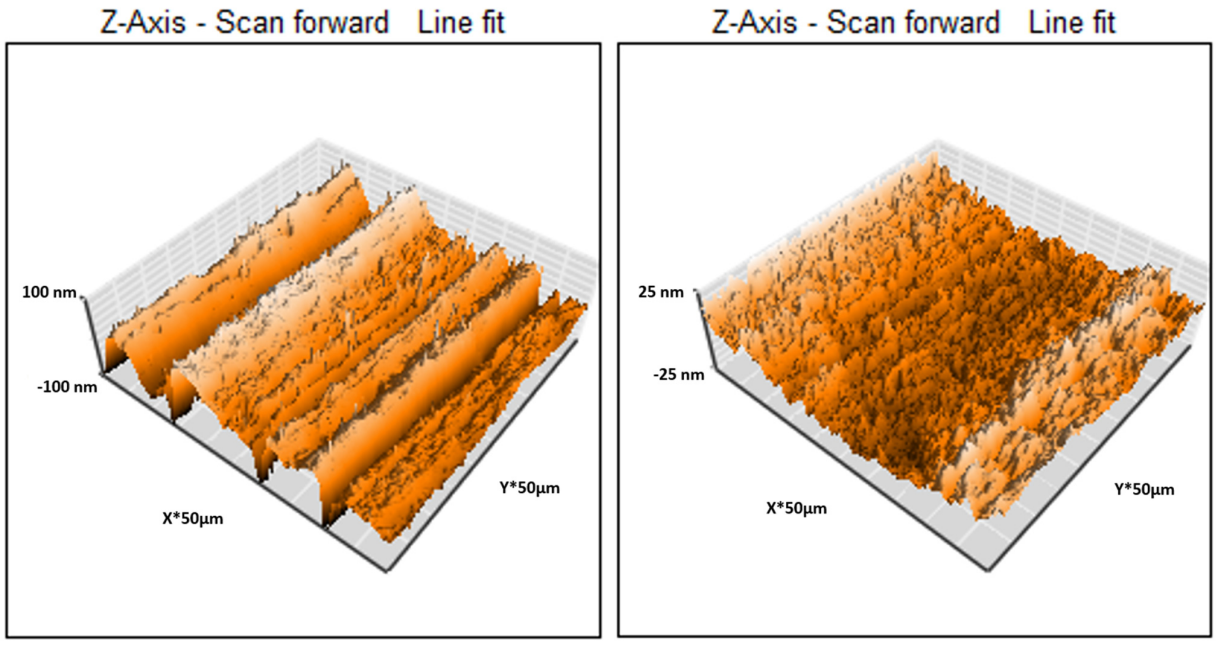

(**a**) (**b**)

Figure 6. AFM surface topographic micrograph of the worn surface for untreated (**a**) and treated (**b**) high-strength Ni-Cr steel.

The results of nanoindentation in Figure 7a show the hardness and plastic index ratio for the AMF-treated and untreated high-strength Ni-Cr steel, while Figure 7b displays the loading–unloading curve for the treated and untreated conditions. These nanoindentation results show that the nanohardness increased by 6% following AMF treatment. The H/E^2 ratio, is an indication of the resistance to plastic deformation and increased by 8% following AMF treatment. This increase suggests that the sample had greater resistance to plastic deformation and wear as a consequence of the AMF treatment.

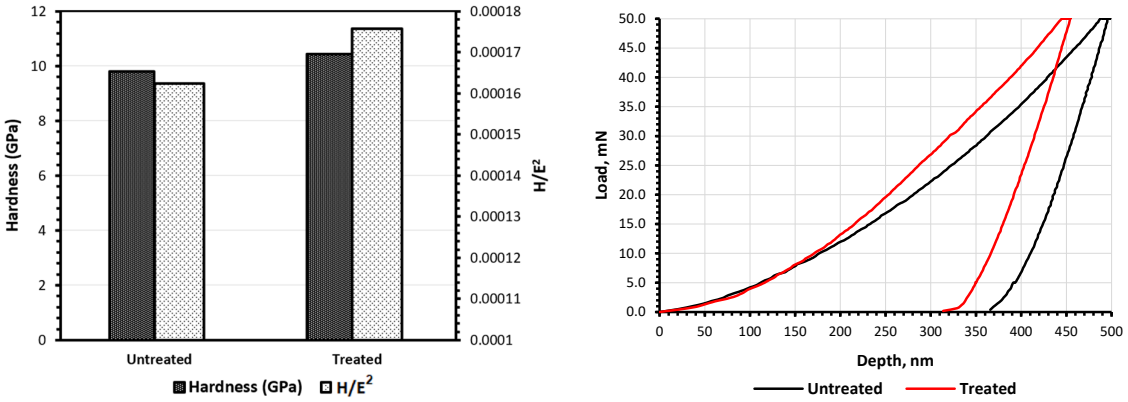

(**a**) (**b**)

Figure 7. Nanoindentation results of (**a**) hardness and H/E^2 and (**b**) loading–unloading curves of treated and untreated high-strength Ni-Cr steel.

The results of the XRD phase analyses for the untreated and AMF-treated high strength Ni-Cr steel are presented in Figure 8. A drop in the XRD peak intensities of austenite following the AMF treatment is apparent. Using the Topas 6 software and Rietveld refinement, it was determined that the AMF treatment caused an increase in the martensitic phase of 0.51% by transformation from austenite. Small amounts of austenite were reported to transform into martensite by other studies [18,26] by exposure to high magnetic fields. The increase in the amount of martensite was accompanied by an increase in the microhardness and nanohardness and in improved wear resistance for the AMF-treated samples.

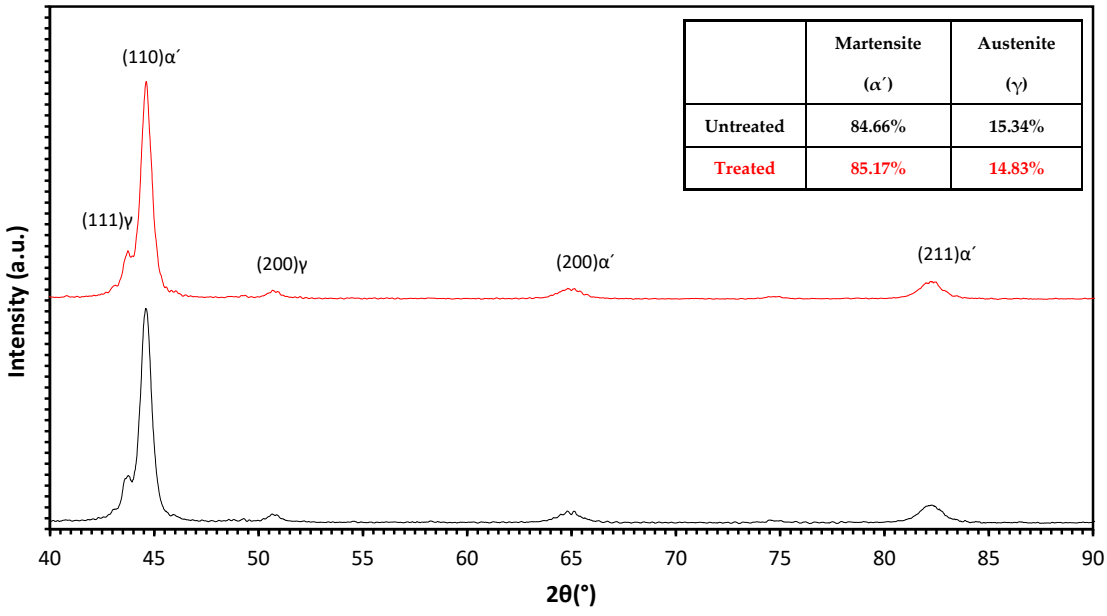

	Martensite (α′)	Austenite (γ)
Untreated	84.66%	15.34%
Treated	85.17%	14.83%

Figure 8. X-ray diffraction patterns of untreated (black) and AMF-treated (red) specimens of high-strength Ni-Cr steel.

4. Discussion

An inspection of Figure 5b shows evidence of surface deformation and the formation of pits during the pin-on-disc test for the untreated sample along with wide wear tracks. The amount of deformation for the AMF-treated sample was less with less wide wear tracks, but there was no evidence of pitting, as presented in Figure 5d. No cracks were observed for either sample. The topographical evidence presented in Figure 6, shows that the asperities for the untreated sample were much higher in comparison with the asperities for the AMF-treated sample. The higher hardness and compressive residual stresses for the AMF-treated samples are likely to hinder deformation, resulting in the formation of asperities of lower height and in a smoother operation with a lower COF value as the sliding pin moves against the 20Cr2Ni4A alloy. The higher asperities for the untreated alloy experienced higher contact pressures, and this resulted in greater surface damage in the form of peeling pits, possibly due to delamination in areas where austenite (which is softer than martensite) was probably present; as the pin-on-disc test proceeded, the COF against time plot was not as smooth as that for the AMF-treated samples. An almost steady-state was established with occasional increases due to material removal. Figure 4a shows that the COF value for the AMF-treated 20Cr2Ni4A alloy decreased with time. This may be attributed to the formation of a protective oxide layer, leading to lower friction [27,28].

The observed improvement in the wear resistance of 20Cr2Ni4A was the result of an increase in the microhardness and nanohardness of the alloy following the application of AMF treatment. This improvement in the hardness properties and wear behaviour can be attributed to various factors including the increase in the amount of martensite in the 20Cr2Ni4A high-strength Ni-Cr steel by transformation from the retained austenite. The phase transformation took place by the application of AMF treatment for an exposure period of 30 min using simple and inexpensive equipment. If AMF treatment is to be fully developed into a useful processing technique, it is important to understand the role of the magnetic field in causing phase transformations. The most common variables that are used in processing and in the description of the chemical thermodynamic state of a material are composition, temperature and pressure. The pressure and elemental composition were not varied during the treatment; therefore, the first possible cause to consider that could have resulted in the observed increase in the amount of martensite is the effect of temperature and, more specifically, the possibility of the alloy being heated during the AMF treatment followed by its cooling at the end of the process. The 20Cr2Ni4A alloy steel used in the present study contained 3.41% Ni by weight; based on research by Tanaka et al. [29], in Fe-Ni alloys containing low amounts of Ni (below about 6 wt.%), martensite starts to form during cooling at a martensite start, M_s, temperature of around 350 °C. A possible influential factor when applying an alternating magnetic field is the generation of eddy currents that are induced within the alloy. As the polarity of the magnetic field was altered every 5 s during the AMF treatment, eddy currents were induced and could have resulted in heating within the specimens to activate microstructural changes. As stated earlier, the average temperature increase that was measured during the AMF treatment was only 15.2 °C, and this was followed by cooling. Clearly, the temperature of the alloy during the AMF treatment always remained well below the M_s temperature and, therefore, there was no transformation to austenite during heating. In any case, even if there was a transformation to austenite followed by cooling to martensite, it is well known that there exists a hysteresis in the temperature dependence of martensitic transformations [30,31] and, therefore, a heating-cooling cycle would not cause any change in the phase composition. To avoid any caused effects by temperature increase, XRD scans were conducted in a temperature-controlled environment (21 °C). The reason for the transformation of more martensite must lie elsewhere. In their classic book on chemical thermodynamics, Lewis and Randall [32]

recognised that other independent parameters like magnetic and electric fields can be variables that contribute to the chemical thermodynamic properties of a material. The effect of a magnetic field on the α/Υ phase relationship in the Fe-Si equilibrium system was studied by Gao et al. [33], who used computational phase diagram predictions to show significant differences in the α/Υ transformation temperature as the magnetic field strength increased. Specifically, the ferromagnetic α phase field was observed to enlarge while the paramagnetic Υ phase decreased as the magnetic flux density increased. From the reported observations, it is apparent that changes in the magnetic flux density can significantly affect phase transformations; it can be deduced that increases in magnetic flux density can favour transformation to ferromagnetic phases, while non-magnetic phases can become less stable. Based on this evidence [32], the application of an external magnetic field can make an additional contribution to the Gibbs Free energy, ΔG°, as presented in Equation (5),

$$\Delta G^{\circ} = \Delta G^{\circ}{}_{non-magnetic} + \Delta G^{\circ}{}_{magnetic\ (internal)} + \Delta G^{\circ}{}_{magnetic\ (external)} \quad (5)$$

which shows an external magnetic contribution in addition to an internal magnetic contribution and a non-magnetic contribution. The application of an external magnetic field will not affect the level of the non-magnetic and internal magnetic contributions, but it will, of course, extend the external magnetic contribution, which can be determined from Equation (6):

$$\Delta G^{\circ}{}_{magnetic\ (external)} = -\mu \int_0^H M\, dH \quad (6)$$

where M represents the magnetisation, H stands for the magnetic flux density and μ is the vacuum permeability (also known as the magnetic constant). The AMF treatment leads to an increase in the magnetic flux density, H; the negative sign on the right-hand side of Equation (6) means that the external magnetic contribution to the Free energy is negative, and according to Equation (5), the overall Gibbs Free energy will become more negative. Both austenite and martensite can be described as metastable phases, with the latter forming as the former is cooled down. The more negative Gibbs Free energy that resulted from the application of the higher magnetic flux density during the AMF treatment provided the thermodynamic driving force to transform more of the retained austenite to martensite. An additional factor contributing to this change is the fact that martensite is ferromagnetic, and its presence would have been promoted at the expense of the paramagnetic austenite as a result of magnetisation due to the treatment. Results from a recent study by Zhu et al. [34], who tempered M50 bearing steel at temperatures between 300 °C and 540 °C in the presence of an alternating magnetic field of a maximum magnetic flux density of 0.1 T, seem to support this suggestion. These authors [34] showed evidence of higher levels of austenite transforming to martensite when tempering was conducted simultaneously with an AMF treatment. The tempering of M50 steel over a similar range of temperatures under a constant magnetic flux density of 12 T has been observed to also lead to transformation of retained austenite to ferrite [35] which is ferromagnetic. However, it must be stressed that in the present study, the transformation was observed at very close to room temperature. Fundamental studies [36] on austenite-to-martensite transformations have shown that transformations below the M_s temperature occur at a rapid rate. Since the AMF treatment was performed at room temperature, the driving force to establish the new equilibrium state following the AMF treatment was large and the transformation to an additional amount of martensite was expected to be fast.

The results of the present study show that application of an alternating magnetic field can lead to changes related to residual stress (and strain). The XRD analysis showed that the surface residual stresses became more compressive after the AMF treatment and that such changes could also have been influenced by the non-magnetic contribution of

the Gibbs Free energy. The generation of a higher level of surface compressive residual stress is another factor that can lead to improved wear resistance. This is desirable in materials for bearing applications as higher compressive stresses will not only increase the wear resistance but will also inhibit crack initiation and improve resistance to fatigue. The increase in surface compressive residual stresses following AMF treatment can be related to dislocation movement. In previous work on ferrous alloys, the authors of the present study [13,37,38] used transmission electron microscopy (TEM) to demonstrate the movement of dislocations due to AMF treatment. Microstructural changes involving phase changes and dislocation movement are normally activated by heating. However, measurements of temperature during the AMF treatment recorded a temperature increase of only 15.2 °C, which is very low and would have been unable to induce any substantial dislocation movement. Therefore, a factor other than temperature was responsible for the observed change in residual stress. Earlier research [39,40] has shown that the movement of dislocations and subsequent changes in residual stresses can take place by the application of external fields where the electric current density exceeds a threshold value of about 1×10^8 A/m^2.

The numerical modelling using Quickfield software showed that the 20Cr2Ni4A high-strength Ni-Cr steel sample experienced a magnetic flux density of approximately 2.58 T during the AMF treatment as it became magnetised under the influence of the external magnetic field. Figure 9 displays the distribution of maximum eddy currents along the cylindrical flat surface of the sample at the point when the polarity changes. The results indicate that altering the external magnetic field polarity induced eddy currents at the flat surface of the sample with a peak current density of 2.75×10^6 A/m^2 near the outer radius. However, this value is almost two orders of magnitude below the current density that must be exceeded to achieve dislocation movement in metals. Therefore, a mechanism other than eddy current heating was responsible for dislocation movement.

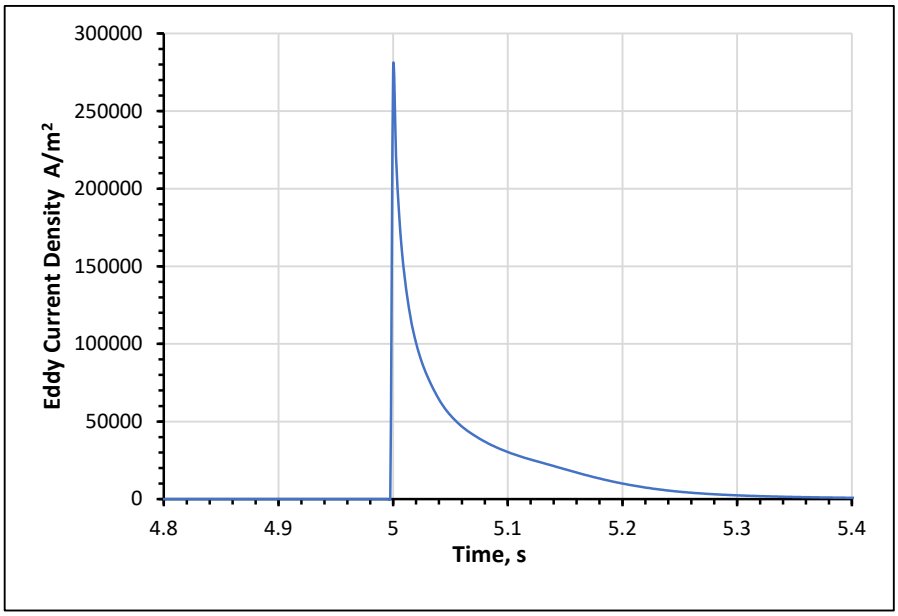

Figure 9. Calculation using QuickField 6 software of the eddy current density at the cylindrical surface of the sample.

The simulation results showed that the value of the magnetic flux density that was used to treat the high-strength Ni-Cr steel samples was 2.58 T, a value that is large enough for martensite to reach a state of magnetic saturation. When in this state, martensite experiences displacement of the magnetic domain walls. As a result, the individual magnetic

moments in atoms become aligned with each other and are thus pointed in the same direction. The consequence of this was to create a single-domain structure. At the instant when the magnetic field alternates, the magnetic flux density decreases to zero. This is followed by an increase in the magnetic flux density of an opposite polarity. This causes the displacement of the magnetic domain walls; this is again accompanied by the creation of a single-domain structure when magnetic saturation is reached. This process is repeated throughout the AMF treatment. Dislocations act as pinning sites for magnetic domain walls and also serve as barriers to their movement [41]. When the magnetic flux density becomes high enough, an abrupt movement of the magnetic domain walls takes place to by-pass the dislocations, and this is recorded as Barkhausen noise [42]. The displacement of the magnetic domain walls causes the depinning of dislocations, and this is the main mechanism that leads to increased dislocation mobility. By interacting with the magnetic domain walls, dislocations are enabled to overcome obstructions and barriers within the crystal lattice. Displacement of the magnetic domain walls due to an increase/decrease in and the rotation of the domain walls causes the depinning of dislocations; this is commonly suggested as the primary mechanism that leads to increased dislocation mobility when ferromagnetic metals are magnetically treated [14,43–45]. The magnetostriction of martensite during magnetisation is another factor that triggers dislocation depinning, thus allowing dislocation movement [43,44]. The movement of dislocations, as stimulated by the AMF treatment, can lead to the annihilation of some dislocations of the opposite sign. In addition, the electric current (eddy current) can cause dislocations to move towards the sample surface, which acts as a natural sink for dislocations, as demonstrated experimentally using a transmission electron microscope by Vdovin and Kasumov [46]. As dislocations migrate towards the surface, micro-strains are accumulated in the subsurface, areas providing an increase in surface compressive residual stresses as well as an increase in surface hardness [47,48].

The increase in a higher level of compressive residual stresses is also influenced by the austenite-to-martensite phase transformation. The state and magnitude of the residual stress in the untreated as-received high-strength Ni-Cr steel is dependent on the expansion that takes place during the austenite-to-martensite transformation (due to the lower density of martensite) and to the thermal contraction while the material is being cooled during manufacturing [49]. In conventional treatment, which involves heating followed by cooling, the volume expansion during the formation of martensite leads to an increase in compressive residual stresses, but some of this effect is lost during cooling due to thermal shrinkage. High and medium M_s temperatures (as exhibited by the high-strength Ni-Cr steel) tend to reduce the effect of transformation-induced compressive residual stresses because the martensitic expansion at high temperatures is followed by shrinkage during cooling. However, the austenite-to-martensite phase transformation that is induced by AMF treatment takes place near room temperature and is therefore not accompanied by shrinkage (as it is not accompanied by fast cooling). In addition to the movement of dislocations, as discussed above, the observed increase in compressive residual stresses due to AMF treatment is partly caused by the transformation of some of the retained austenite to martensite. The advantage of forming an additional amount of martensite by AMF treatment is the fact that transformation to martensite occurs near room temperature; therefore, it is not accompanied by any thermal shrinkage. The use of the AMF technique as a post-treatment can thus be beneficial in extending the level of compressive residual stresses which form within the alloy because the treatment is not accompanied by any thermal shrinkage.

The overall observed changes are beneficial in that they establish low and more stable friction during the wear tests. The nanoindentation results showed that there was an increase in the plastic index ratio (H/E^2) of 8% following the AMF treatment. The

increase in this ratio typically limited the degree of plastic deformation during the pin-on-disc wear test and hence improved the wear resistance of the alloy. Furthermore, the nanoindentation results showed that the elastic recovery parameter increased by 7.5% due to the AMF treatment. This result suggests that when the treated alloy underwent pin-on-disc testing, a higher ratio of elastic contact occurred and this resulted in lower adhesion and in a lower friction coefficient between the contacting surfaces. Low and more stable friction was therefore evident, leading to lower wear loss during the pin-on-disc wear tests. The observed results are of importance for sliding contact bearing applications because the AMF treatment is shown to improve the wear resistance of the 20Cr2Ni4A alloy and would thus extend its lifetime. The lower amount of damage that was observed during the sliding contact pin-on-disc tests would also have been effective in providing sliding fatigue resistance. It is vital that research on this line of enquiry continues so that the AMF process can be widely applied commercially. The process has the potential to replace heat-treatment as a processing technique, but for that to be achieved, equilibrium phase diagrams of magnetic flux density against composition are needed. Furthermore, commercial equipment capable of producing higher levels of magnetic flux density has to be developed so that high current densities can be achieved for processing large components.

5. Conclusions

The reported study has shown that AMF treatment can be used as a process to extend the wear and friction behaviour of 20Cr2Ni4A high-strength Ni-Cr alloy steel. The following conclusions can be drawn:

1. AMF treatment yielded a decrease in the specific wear rate of high-strength Ni-Cr steel by 58%, in the wear scar width by 23%, in the surface roughness by 69% and in the coefficient of friction by 28%, as observed from the pin-on-disc test results. These observations were attributed to an increase in the nano- and microhardness of the alloy caused by an increase in the amount of martensite and by the presence of higher surface compressive residual stresses.
2. The application of the alternating magnetic field made an external magnetic field contribution that led to a decrease in ΔG° and caused the additional precipitation of martensite from the retained austenite at ambient temperature.
3. The increase in the surface compressive residual stress was attributed to two factors:
    - The movement of dislocations towards the surface of the high-strength Ni-Cr alloy steel samples, creating micro-strains in the subsurface regions;
    - The expansion that accompanied the austenite-to-martensite transformation at ambient temperature (in the absence of any thermal cooling and any shrinkage).
4. The increase in temperature during the AMF treatment was very small (15.2 °C), while the induced current density was about two orders of magnitude below the value required for dislocation movement.
5. The main mechanism of dislocation movement at ambient temperature was the movement of magnetic domain walls and magnetostriction as the magnetic field alternated, causing the depinning and movement of dislocations.

Author Contributions: Conceptualisation, S.A., A.B. and A.C.; methodology, S.A., M.B., A.B. and A.C.; validation, A.B.; formal analysis, S.A., M.B., A.B. and A.C.; investigation, S.A. and A.B.; resources, A.C.; data curation, S.A. and A.B.; writing—original draft, S.A., M.B., A.B. and A.C.; writing—review and editing, S.A., M.B., A.B. and A.C.; supervision, A.B. and A.C.; project administration, A.B. and A.C.; funding acquisition, A.B. and A.C. All authors have read and agreed to the published version of the manuscript.

Funding: This research was supported by the Marie Curie International Incoming Fellowship scheme within the 7th European Commission Framework Programme Grant, number PIIF-GA-2010-274324.

Data Availability Statement: The original contributions presented in the study are included in the article, further inquiries can be directed to the corresponding author.

Conflicts of Interest: The authors declare no conflict of interest.

References

1. Luo, Q.; Kitchen, M.; Patel, V.; Magowan, S. Carbon partitioning and structure evolution in the hardening treatments of high strength steel. In Proceedings of the 20th Congress of International Federation for Heat Treatment and Surface Engineering, Beijing, China, 23–25 October 2012.
2. Luo, Q. A new XRD method to quantify plate and lath martensites of hardened medium-carbon steel. *J. Mater. Eng. Perform.* **2016**, *25*, 2170–2179. [CrossRef]
3. Shao, Q.; Kang, J.; Xing, Z.; Wang, H.; Huang, Y.; Ma, G.; Liu, H. Effect of pulsed magnetic field treatment on the residual stress of 20Cr2Ni4A steel. *J. Magn. Magn. Mater.* **2019**, *476*, 218–224. [CrossRef]
4. Huo, Z.; Zhang, Y.; Jombo, G.; Shu, L. Adaptive Multiscale Weighted Permutation Entropy for Rolling Bearing Fault Diagnosis. *IEEE Access* **2020**, *8*, 87529–87540. [CrossRef]
5. Zhang, Y.; Bingham, C.; Martínez-García, M.; Cox, D. Detection of emerging faults on industrial gas turbines using extended Gaussian mixture models. *Int. J. Rotating Mach.* **2017**, *2017*, 5435794. [CrossRef]
6. Shiozawa, K.; Lu, L. Very high-cycle fatigue behaviour of shot-peened high-carbon–chromium bearing steel. *Fatigue Fract. Eng. Mater. Struct.* **2002**, *25*, 813–822. [CrossRef]
7. Jeddi, D.; Lieurade, H.-P. Effect of retained austenite on high cycle fatigue behavior of carburized 14NiCr11 steel. *Procedia Eng.* **2010**, *2*, 1927–1936. [CrossRef]
8. Nélias, D.; Jacq, C.; Lormand, G.; Dudragne, G.; Vincent, A. New Methodology to Evaluate the Rolling Contact Fatigue Performance of Bearing Steels With Surface Dents: Application to 32CrMoV13 (Nitrided) and M50 Steels. *J. Tribol.* **2005**, *127*, 611–622. [CrossRef]
9. Kobs, K.; Dimigen, H.; Denissen, C.J.M.; Gerritsen, E.; Politiek, J.; van Ijzendoorn, L.J.; Oechsner, R.; Kluge, A.; Ryssel, H. Friction reduction and zero wear for 52100 bearing steel by high-dose implantation of carbon. *Appl. Phys. Lett.* **1990**, *57*, 1622–1624. [CrossRef]
10. Hetzner, D.W. Refining carbide size distributions in M1 high speed steel by processing and alloying. *Mater. Charact.* **2001**, *46*, 175–182. [CrossRef]
11. Babutskyi, A.; Mohin, M.; Chrysanthou, A.; Xu, Y.; Lewis, A. Effect of electropulsing on the fatigue resistance of aluminium alloy 2014-T6. *Mater. Sci. Eng. A* **2020**, *772*, 138679. [CrossRef]
12. Mohin, M.A.; Toofanny, H.; Babutskyi, A.; Lewis, A.; Xu, Y.G. Effect of Electromagnetic Treatment on Fatigue Resistance of 2011 Aluminum Alloy. *J. Multiscale Model.* **2016**, *7*, 1650004. [CrossRef]
13. Akram, S.; Babutskyi, A.; Chrysanthou, A.; Montalvão, D.; Pizurova, N. Effect of Alternating Magnetic Field on the Fatigue Behaviour of EN8 Steel and 2014-T6 Aluminium Alloy. *Metals* **2019**, *9*, 984. [CrossRef]
14. Çelik, A.; Yetim, A.F.; Alsaran, A.; Karakan, M. Effect of magnetic treatment on fatigue life of AISI 4140 steel. *Mater. Des.* **2005**, *26*, 700–704. [CrossRef]
15. Tang, Y.; Hosoi, A.; Morita, Y.; Ju, Y. Restoration of fatigue damage in stainless steel by high-density electric current. *Int. J. Fatigue* **2013**, *56*, 69–74. [CrossRef]
16. Wang, Y.; Xing, Z.; Huang, Y.; Guo, W.; Kang, J.; Wang, H.; Zhang, Z. Effect of pulse magnetic field treatment on the hardness of 20Cr2Ni4A steel. *J. Magn. Magn. Mater.* **2021**, *538*, 168248. [CrossRef]
17. Yetim, A.; Kovacı, H.; Aslan, M.; Çelik, A. The effect of magnetic field on the wear properties of a ferromagnetic steel. *Wear* **2013**, *301*, 636–640. [CrossRef]
18. Babutskyi, A.; Chrysanthou, A.; Zhao, C. Effect of pulsed magnetic field pre-treatment of AISI 52100 steel on the coefficient of sliding friction and wear in pin-on-disk tests. *Friction* **2014**, *2*, 310–316. [CrossRef]
19. Snegovskij, F.; Uvarov, V.A. The influence of magnetic treatment of screw propeller on the cavitation wear. *Trenie Iznos* **1991**, *12*, 535–539.
20. Hiratsuka, K.; Sasada, T. Wear of metals in a magnetic field. *Wear* **1993**, *160*, 119–123. [CrossRef]
21. Xi, X.; Xia, Y.; Hu, Y. The Effects of Magnetic Treatment on the Tribological Behavior of AISI 1045 Steel under Lubricated Conditions. *Tribol. Trans.* **2018**, *61*, 671–682. [CrossRef]
22. Bhaumik, S.; Pathak, S. A Comparative Experimental Analysis of Tribological Properties Between Commercial Mineral Oil and Neat Castor Oil using Taguchi Method in Boundary Lubrication Regime. *Tribol. Ind.* **2016**, *38*, 33–44.

23. *ASTM 99-95a*; Standard Test Method for Wear Testing with a Pin-on-Disk Apparatus. ASTM International: West Conshohocken, PA, USA, 2000.
24. Cseh, D.; Mertinger, V. X-Ray Diffraction Measurements of Residual Stress Induced by Surface Compressing Methods. *Mater. Sci. Forum* **2012**, *729*, 199–204.
25. Magweb, Free BH Curves—Magweb. Magweb. Available online: https://www.magweb.us/ (accessed on 1 December 2024).
26. Pappas, N. Calculating retained austenite in steel post magnetic processing using X-ray diffraction. *BS Undergrad. Math. Exch.* **2006**, *4*, 8–14.
27. Ralls, A.M.; Leong, K.; Liu, S.; Wang, X.; Jiang, Y.; Menezes, P.L. Unraveling the friction and wear mechanisms of surface nanostructured stainless-steel. *Wear* **2024**, *538*, 205185. [CrossRef]
28. Zhang, Y.; Hou, W.; Yu, J.; Chen, C.; Zhou, L. The role of carbon in wear resistance of CoCrFeNiTi0. 5 high-entropy alloy layer. *J. Mater. Eng. Perform.* **2024**, 1–13. [CrossRef]
29. Tanaka, M.; Choi, C.S.; Kojima, Y. Effect of Ms Temperature on Strength and Toughness in Martensitic Fe-Ni-C Alloys. *Trans. Iron Steel Inst. Jpn.* **1974**, *14*, 110–117. [CrossRef]
30. Kaufman, L.; Cohen, M. The martensitic transformation in the iron-nickel system. *JOM* **1956**, *8*, 1393–1401. [CrossRef]
31. Burkart, M.W.; Read, T. Diffusionless phase change in the indium-thallium system. *Trans. Am. Inst. Min. Metall. Eng.* **1953**, *197*, 1516–1524.
32. Lewis, G.N.; Randall, M. *Thermodynamics and the Free Energy of Chemical Substances*; McGraw-Hill: New York, NY, USA; London, UK, 1923.
33. Gao, M.C.; Bennett, T.A.; Rollett, A.D.; Laughlin, D.E. The effects of applied magnetic fields on the α/γ phase boundary in the Fe–Si system. *J. Phys. D Appl. Phys.* **2006**, *39*, 2890–2896. [CrossRef]
34. Zhu, F.; Jiang, D.; Sun, S.; Wu, H.; Zhang, Z.; Wang, J.; Ren, Z. Effect of alternating magnetic field on microstructure evolution and mechanical properties of M50 bearing steel during tempering process. *J. Mater. Res. Technol.* **2023**, *26*, 4516–4525. [CrossRef]
35. Wang, F.; Qian, D.; Hua, L.; Mao, H.; Xie, L.; Song, X.; Dong, Z. Effect of high magnetic field on the microstructure evolution and mechanical properties of M50 bearing steel during tempering. *Mater. Sci. Eng. A* **2020**, *771*, 138623. [CrossRef]
36. Machlin, E.; Cohen, M. Burst phenomenon in the martensitic transformation. *JOM* **1951**, *3*, 746–754. [CrossRef]
37. Babutskyi, A.; Akram, S.; Bevilacqua, M.; Chrysanthou, A.; Montalvão, D.; Whiting, M.J.; Pizurova, N. Improvement of cavitation erosion resistance of structural metals by alternating magnetic field treatment. *Mater. Des.* **2023**, *226*, 111630. [CrossRef]
38. Akram, S.; Babutskyi, A.; Chrysanthou, A.; Montalvão, D.; Whiting, M.J.; Modi, O.P. Improvement of the wear resistance of EN8 steel by application of alternating magnetic field treatment. *Wear* **2021**, *484–485*, 203926. [CrossRef]
39. Troitskii, O.A.; Spitsyn, V.I.; Sokolov, N.V.; Ryzhkov, V.G. Application of high-density current in plastic working of metals. *Phys. Status Solidi A* **1979**, *52*, 85–93. [CrossRef]
40. Baranov, Y.V.; Troitskii, O.A.; Avraamov, Y.S.; Shlyapin, A.D. Physical bases of electric-pulse and electroplastic treatments and new materials. *Chap* **2001**, *1*, 56–77.
41. Jiles, D. *Introduction to Magnetism and Magnetic Materials*; CRC Press: Boca Raton, FL, USA, 2015.
42. Fukumoto, Y.; Kamijo, A. Effect of milling depth of the junction pattern on magnetic properties and yields in magnetic tunnel junctions. *Jpn. J. Appl. Phys.* **2002**, *41*, L183. [CrossRef]
43. Tang, G.; Xu, Z.; Tang, M.; Chen, X.; Zhou, H.; Lu, A. Effect of a pulsed magnetic treatment on the dislocation substructure of a commercial high strength steel. *Mater. Sci. Eng. A* **2005**, *398*, 108–112. [CrossRef]
44. Klamecki, B.E. Residual stress reduction by pulsed magnetic treatment. *J. Mater. Process. Technol.* **2003**, *141*, 385–394. [CrossRef]
45. Wu, S.; Zhao, H.; Lu, A.; Fang, H.; Tang, F. A micro-mechanism model of residual stress reduction by low frequency alternating magnetic field treatment. *J. Mater. Process. Technol.* **2003**, *132*, 198–202. [CrossRef]
46. Vdovin, E.; Kasumov, A. Direct observation of electrotransport of dislocations in a metal. *Sov. Phys. Solid State* **1988**, *30*, 180–181.
47. Frankel, J.; Abbate, A.; Scholz, W. The effect of residual stresses on hardness measurements. *Exp. Mech.* **1993**, *33*, 164–168. [CrossRef]
48. Jang, J.I. Estimation of residual stress by instrumented indentation: A review. *J. Ceram. Process. Res* **2009**, *10*, 391–400.
49. Payares-Asprino, M.; Katsumoto, H.; Liu, S. Effect of martensite start and finish temperature on residual stress development in structural steel welds. *Weld. J.* **2008**, *87*, 279s–289s.